## Evidence of crustal melting events below the Island of Salina (Aeolian Atc, Southern Italy)

Zavon, V.; Nikogosian, I.

***published in***
Geological Magazine
2004

***DOI (link to publisher)***
10.1017/S0016756804009124

***document version***
Publisher's PDF, also known as Version of record

*Geol. Mag.* **141** (*4*), *2004, pp. 525–540. © 2004 Cambridge University Press*
DOI: 10.1017/S0016756804009124 *Printed in the United Kingdom*


# Evidence of crustal melting events below the island of Salina (Aeolian arc, southern Italy)

V. ZANON* & I. NIKOGOSIAN†

*Istituto Nazionale di Geofisica e Vulcanologia, Piazza Roma, 2, I-95123 Catania, Italy
†Faculty of Geosciences, Utrecht University, Budapestlaan 4, 3584 CD Utrecht, Netherlands; and Faculty of Earth and Life Sciences, Vrije Universiteit, De Boelelaan 1085, 1081 HV Amsterdam, Netherlands

(*Received* 10 March 2003; *accepted* 23 December 2003)

**Abstract** – Quartz-rich xenoliths hosted in the basaltic–andesitic and andesitic lavas of Monte dei Porri, in the island of Salina, contain fluid and melt inclusions whose study makes it possible to trace back the magma ascent path of this volcano; moreover, they are a source of information about the anatectic processes that occurred under this island. The texture, mineralogy and whole-rock chemistry of these rocks exhibit the typical characteristics of a residual rock which went through several melt extraction events. The chemistry of melt inclusions hosted inside quartz grains ($SiO_2 > 72.7\%$, $Al_2O_3 = 9.0$–$13.5\%$, $CaO = 0.2$–$4.3\%$, $K_2O > 3.1\%$, MgO, $FeO_t \leq 1.5\%$) supports the hypothesis that a progressive and continuous anatectic processes affected a peraluminous high-grade metamorphic rock (gneiss or micaschist), that constituted the Calabro–Peloritani basement and generated a quartz-bearing residue. The fluids trapped inside these inclusions are rarely composed of high-density $CO_2$, with a homogenization temperature to liquid phase ($Th_L$) within the range 26.2–31.0 °C, corresponding to densities of 520 to 690 kg/m$^3$. More commonly, they are made up of low-density $CO_2$, with a homogenization temperature to vapour phase ($Th_V$) within the range 13.2–31.0 °C, corresponding to density values of 150 to 460 kg/m$^3$. It is proposed that, during ascent, batches of magma rising from the mantle sampled various fragments of a residual rock from a depleted metamorphic basal layer and carried them to the surface. Magmas probably stopped inside at least two distinct reservoirs located at different depths ($\leq 12.7$ km and between 1.7 and 4.7 km), in which they underwent fractional crystallization. The ascent speed of the xenolith-bearing magmas from the deeper storage area to the shallower reservoir was fairly high, as confirmed by the low number of high-density fluid inclusions preserved that show re-equilibration features, and by the contemporaneous presence of denser cumulitic Ol + Cpx ± Opx xenoliths in the host lava.

Keywords: melts, anatexis, Aeolian Islands, magma transport, inclusions.

## 1. Introduction

It is commonly thought that all the erupted magmas of the Aeolian arc, even the most primitive ones, were affected to different extents by interaction with crustal rocks through Assimilation and Fractional Crystallization (AFC) or Assimilation and Equilibrium Crystallization (AEC) processes (Esperança *et al.* 1992; Peccerillo & Wu, 1992; Francalanci *et al.* 1993; Clocchiatti *et al.* 1994; De Astis *et al.* 1997, 2000; Gertisser & Keller, 2000; Santo, 2000; Calanchi *et al.* 2002; Gioncada *et al.* 2003). This is partially confirmed by the presence of a great number of crustal xenoliths of various kinds in the volcanic products of this area, especially in the less evolved lavas (Keller, 1974; Peccerillo & Wu, 1992; Francalanci & Santo, 1993; Renzulli *et al.* 2001; Vaggelli *et al.* 2003; Zanon, Frezzotti & Peccerillo, 2003). Some of these, mostly composed of quartz, are chiefly found in the mafic lavas of all the Aeolian Islands and show the same petrological and geochemical features. For this reason, it is very important, especially from a 'regional point of view', to make a detailed study of these rocks, aiming at a definition of their genetic processes.

In the island of Salina, the basaltic andesites and the andesites erupted from Monte dei Porri contain a relevant amount of xenoliths, while these are very scarce or lacking in the dacites and in the lavas erupted by other vents in the island.

The aim of this work is to outline the history of these xenoliths, to define the accumulation/storage depths of the magmas in which they are contained and to demonstrate the occurrence of progressive crustal melting processes. These objectives have been achieved through the study of the textural characteristics of several sampled xenoliths and through the analysis of the chemical composition of the melt inclusions trapped inside the crystals that constitute the xenoliths.

## 2. Geological setting

The island of Salina is located in the southern Tyrrhenian Sea, in the middle of the Aeolian Archipelago,

* Author for correspondence: zanon@ct.ingv.it

on a 18–25 km thick continental crust belonging to the Calabro–Peloritani basement that largely consists of metasedimentary and meta-igneous rocks and Hercynian and pre-Hercynian granitic and metamorphic rocks of various grades (Rottura *et al.* 1991; Van Dijk & Scheepers, 1995). The volcanic activity here may be related to the presence of a NW-dipping Benioff plane, located in the Ionian Sea, that formed during the collision of the African and the European plates (Ellam *et al.* 1989). Other authors suggest that the subduction process ceased about 1 Myr ago and maintain that Aeolian volcanism is a consequence of two events, namely (1) the post-subduction extensional movement caused by slab detachment and sinking beneath the Calabro–Peloritani range (Hyppolite, Angelier & Roure, 1994; Milano, Vilardo & Luongo, 1994; Carminati *et al.* 1998) and (2) by the opening of the southernmost part of the Tyrrhenian Sea (Crisci *et al.* 1991).

The island of Salina lies along a NNW–SSE-oriented graben-like structure (Barberi *et al.* 1994), whose main discontinuity is represented by the dextral strike-slip 'Tindari–Letojanni', that is, the extension of the Maltese Escarpment into the Tyrrhenian Sea (Fabbri, Ghisetti & Vezzani, 1980). This fault is considered to be the determining factor for the rejuvenation of the eruptive activity in this area and, in particular, for the last explosive eruptive stage at Pollara (Lanzafame & Bousquet, 1997).

Salina Island includes the products of six different volcanic centres, which erupted in two distinct periods (Gertisser & Keller, 2000) (Fig. 1). During the first eruptive period (430–127 ka), the explosive centres of Corvo, Capo and Rivi formed. The stratovolcano of Fossa delle Felci was built up at the end of this stage. The chemistry of these lavas and pyroclasts ranges from basalt to dacite.

After a period of erosion and of conglomerate deposition (Tyrrhenian period) volcanic activity resumed at 67 ka at Monte dei Porri and continued until 13 ka, including two explosive eruptions at Pollara vent.

The erupted volcanic rocks, ranging from basalts to rhyolites, belong to the calc-alkaline and the high-K calc-alkaline series. Basaltic-andesite and andesite lava flows constitute the most widespread lithology and sometimes contain quartz-rich xenoliths, whose presence was noted by several other authors (Honnorez & Keller, 1968; Gertisser & Keller, 2000), who hypothesized a crustal origin for these products.

## 3. Analytical techniques

Twenty-one quartz-rich xenoliths were collected from the basaltic–andesitic and andesitic lavas of Monte dei Porri, as they hardly occur in the products of other volcanic cycles. In order to collect xenoliths in their entirety, preserving them as much as possible from the mechanical shock and crushing caused by the sledgehammer, the samples were cored through the use of a portable electric driller.

Only samples of suitable volume and free of lava veinlets were chosen for chemical analysis, sometimes by hand-picking; thereafter, they were cleaned with bi-distilled water and dried in an oven at 110 °C.

Whole-rock analyses of these quartz-rich xenoliths were performed by XRF, on pressed pellets, at the Dipartimento di Scienze della Terra, Università di Perugia, using a Philips PW 1400 X-ray fluorescence spectrometer. Correction for matrix effects was applied following Franzini & Leoni (1972) and Kaye (1965). Precision is higher than 15% for V, Cr, Ni, higher than 10% for Co, Cr, Y, Zr, Ba, and higher than 5% for all the other elements. Accuracy was tested on international standards and is greater than 10%.

$Na_2O$, MgO, and LOI (Loss On Ignition) were determined through wet chemical analyses utilizing atomic absorption spectrophotometry. Rare Earth Element (REE) concentrations in the xenoliths were determined by ICP-MS at the Centre de Recherches Pétrographiques et Géochimiques, CNRS, Nancy, France. Precision is greater than 15% for Cr, Cu, La and Sm, greater than 10% for Ba, Ce, Ga, Hf, Pb, Sr, Ta, V and Zr and greater than 8% for Nb, Nd, Rb, Th, U and Y.

Doubly polished, 100–200 μm thick wafers were prepared for the microthermometric study of fluid and melt inclusions and for Raman spectroscopic investigation at the Università di Siena, where a Linkam® THM 600 heating/freezing stage was used to study fluid inclusions. Instrumental error was $\pm 0.1$ °C at the reference standard point and density values and pressures were calculated using the equation of state conceived by Holloway (1981) for $CO_2$.

Raman investigations were performed by means of a confocal Labram multichannel spectrometer built by Jobin-Yvon LTD for the purpose of ascertaining the presence of even a small amount of water. The source of excitation was an $Ar^+$ laser. The beam was focused at a spot size of about 1–2 μm, using an Olympus 100× lens. Raman intensities were measured with a Peltier-cooled CCD detector.

Melt inclusions were homogenized at Vrije Universiteit (VU), Amsterdam, Netherlands, using a fast-quench, high-temperature (1600 °C) heating stage (Sobolev & Slutskii, 1984). Experiments were performed at 1 atm He, purified by a 700 °C Ti exchanger. Temperatures were measured with a Pt–$Pt_{90}Rh_{10}$ thermocouple and controlled by the melting points of gold (1064 °C) and silver (960.8 °C). Each run lasted for 1 to 6 hours due to the high viscosity of the trapped melt, which probably also slowed the process of total homogenization (melting processes were usually completed at a temperature in the range of 35–50 °C, since the first reduction in size of the bubble). The initial heating rate was ~3–5 °C/min up to 900 °C and it then decreased to ~5–30 °C/hour close to homogenization

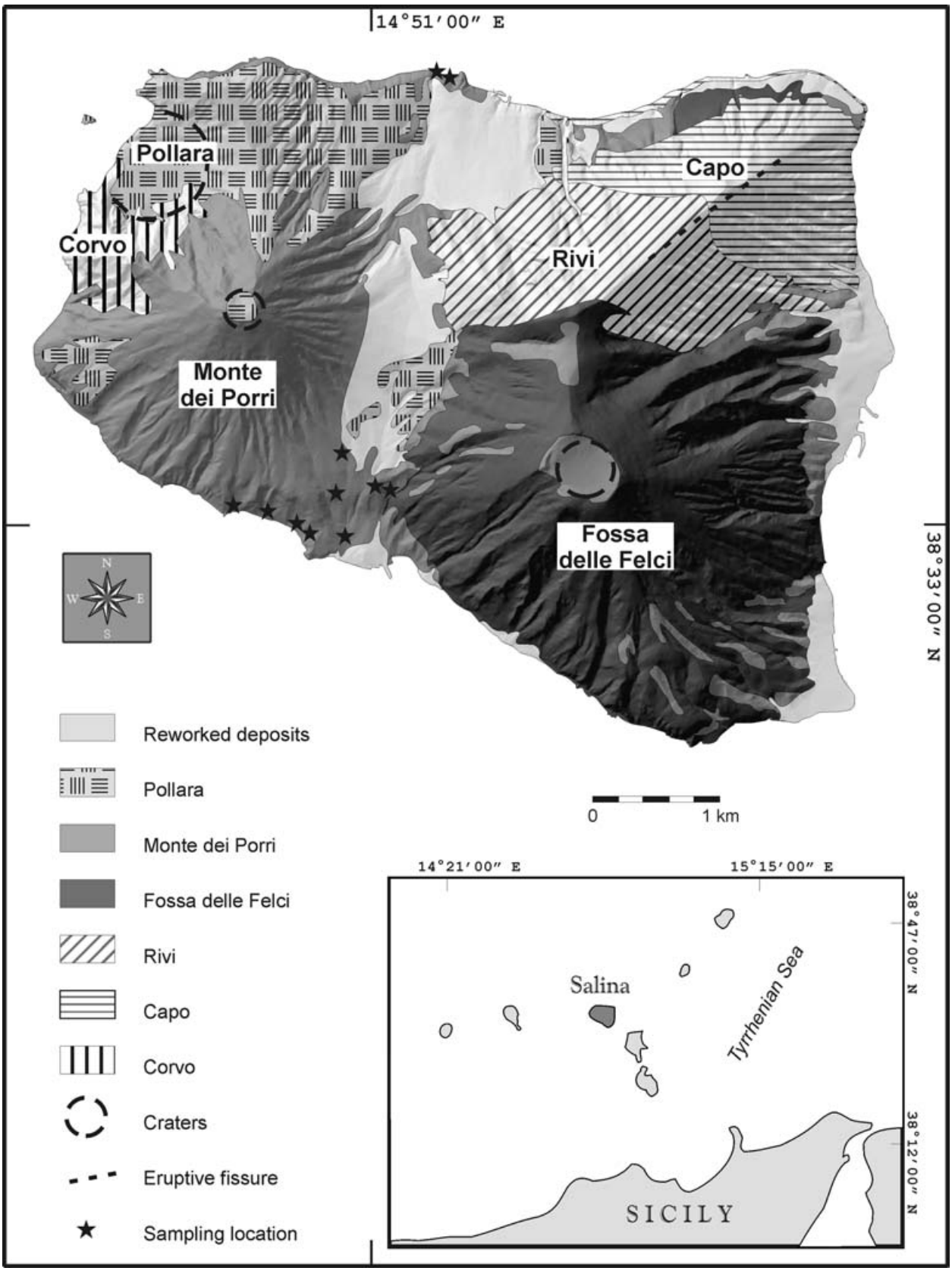


Figure 1. Digital Elevation Model of the island of Salina with superimposed sampling location and geological sketch map.

temperature. Methodological error was estimated to be $\pm 5$–$10\,^{\circ}C$.

Before analysis with the electron microprobe, the grains of quartz with homogenized inclusions were mounted in epoxy, polished to expose the surface of the inclusions, and carbon coated.

Back-scattered photomicrographs and analyses of homogenized melt inclusions of suitable size ($\varnothing \geq 15$ μm) and free of mineral phases were made at VU, using a JEOL Ltd JXA 8800M Superprobe, equipped with four EDS-WDS spectrometers. Analytical conditions were 15 kV for the acceleration voltage and 25 nA for the beam current. Spot sizes were of 2–7 μm, with single-element counting times of 25–50 s on the peak and 10–25 s on the background. Analyses of Mg, Al, Si, Ca and Fe were standardized making reference to the certified JDF-D2#2 MORB standard glass from Lamont-Doherty Earth Observatory, Columbia University, USA. Jadeite and orthoclase were utilized as standards for Na and K, Durango apatite was used for P, marialite for Cl, synthetic $FeTiO_3$ for Ti, synthetic $Mn_2SiO_4$ for Mn, celestine for Sr and synthetic Ba–Al oxide for Ba.

Alkali loss was minimized by measuring with a defocused spot of 2–7 μm, depending on the inclusion size and measuring $Na_2O$ first. The measuring of at least five spots on each major element standard made it possible to check the accuracy, thus allowing the correction of possible systematic errors. Estimated errors for major elements are at least 1–2%. Detection limit for $TiO_2$ and MnO was 0.024%, 0.019% for $P_2O_5$, 0.008% for Cl, 0.033% for SrO and 0.042% for BaO.

## 4. Petrography of the xenoliths and of the hosted melt and fluid inclusions

### 4.a. Xenoliths

The lavas of Monte dei Porri contain xenoliths belonging to distinct lithologies: some comprise magmatic assemblages ($Cpx + Pl \pm Opx$) and show cumulate textures, while others are quartz-bearing rocks. There are also a few shale fragments and thermometamorphic fragments of the basement.

Petrographical and chemical analyses carried out on quartz-bearing xenoliths show that these are constituted almost exclusively of quartz grains and rare feldspars, plus accessory phases (titanite, apatite and zircon). Their shape is always rounded due to the friction with host lava during the flow or the ascent through the conduit (Fig. 2a), and their size ranges from 2–3 cm up to 25–30 cm in diameter. No reaction rims exist at the boundary with lava, but sometimes it is possible to find a network of veinlets of the host lava intruding into the xenoliths and constituting a weakness pattern. Their texture is always granular, with quartz grains varying from rounded to subpolygonal in shape, from transparent to whitish in colour, and measuring from 500 μm to 2 mm (Fig. 2b).

Texturally, it is possible to distinguish two kinds of quartz grains: the first type, called 'Type A', is highly transparent, rounded or irregularly shaped and mostly without fractures (Fig. 2c). It often contains melt inclusions and sometimes tiny trapped phases (chloroapatite, quartz and feldspars). Rare $CO_2$ fluid inclusions are present in this kind of quartz. Grains are often surrounded by a rim of cristobalite (Fig. 2d), as evidenced by back-scattered microphotography and Raman microspectrometry. It is possible to find these grains both isolated and in small clusters, surrounded by the second type of quartz.

The second type, called 'Type B', is poorly transparent and highly fractured, often from rounded to subpolygonal in shape, from white to pale grey in colour and it contains trails of empty fluid inclusions, cross-cutting one another (Fig. 2e).

These two kinds of quartz coexist in xenoliths in different amounts, but on average, the ratio Type-A/Type-B quartz is $\sim$1:10. In a few samples, a thin transparent glassy film surrounds quartz grains of both types, and it sometimes contains tiny (less than 3 μm) trapped crystals of quartz, feldspar and chloroapatite.

### 4.b. Fluid inclusions

Fluid inclusions were found inside both types of quartz grains, but in different amounts: the rarest ones, found only in transparent quartzes, are those represented by small and isolated high-density $CO_2$ bubbles, very often associated with small glass inclusions. The presence of small radial cracks and/or a halo of very small bubbles ($< 2$ μm) is indicative of re-equilibration processes (Andersen & Neumann, 2001; Vityk & Bodnar, 1998). No solid phases were observed inside the cavities. These petrographic features justify the assumption that these inclusions represent an early stage of trapping in the history of the xenoliths.

Low-density $CO_2$-bearing fluid inclusions are more frequent in both types of quartz: isolated or in clusters with rare high-density fluid inclusions and melt inclusions (Fig. 2f) in Type-A quartzes, or isolated or in trails of empty inclusions in Type-B quartzes. They also exhibit re-equilibration features.

### 4.c. Melt inclusions

Perfectly glassy inclusions are common in transparent quartzes, where they are sometimes associated with fluid inclusions and occur isolated or in small clusters. They are colourless and perfectly transparent, their size is less than 60–70 μm and their shape may be either rounded, which is the most common (Fig. 2g), or like that of the negative crystal (Fig. 2h); some other inclusions have an irregular shape, due to the trapping conditions inside small fractures during the latest stages

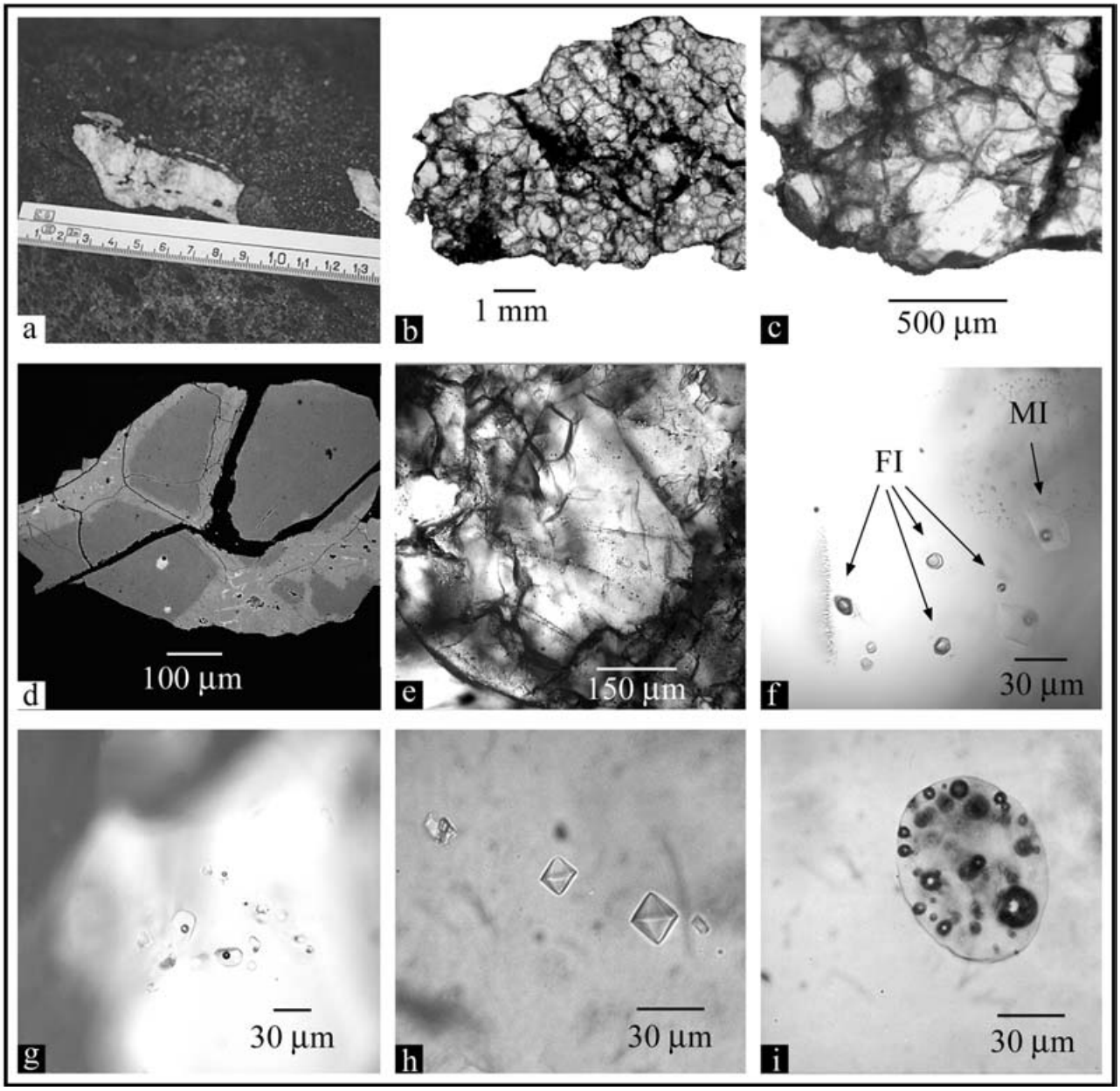


Figure 2. Photomicrographs of xenoliths from the volcano of Monte dei Porri; (a) (SaMp Z) sampled xenolith is composed mainly of quartz grains and there are no reaction rims with the host lava; (b) (SaMp Z) photomicrograph assemblage showing the granular texture of these xenoliths; (c) (SaMp Z) Type-A quartz grain constituting the xenoliths is rounded, highly transparent and with high relief; (d) (Eo98.8) back-scattered image of a grain of Type-A quartz, showing an overgrowth rim of cristobalite. White spots are melt inclusions; (e) (SaMp 13) Type-B quartz grain: trails of late-stage fluid inclusions cross-cutting the grain are well evident; (f) (SaMp 13) cluster of fluid inclusions of critical density, trapped together with some melt inclusions (in the background); (g) (SaMp 5) cluster of rounded silicate melt inclusions of different size, trapped inside a Type-A quartz; (h) (Eo98.8) small trail of melt inclusions with negative-crystal shapes; (i) (Eo98.8) very large inclusion ($Ø \approx 70$ µm) containing a large number of low-density $CO_2$ bubbles, possibly indicating $CO_2$-oversaturation for the melt at the time of trapping.

of evolution. Some of them do not exhibit any shrinkage bubble and lie isolated or in small clusters in the brightest Type-A quartzes. Others, usually the biggest and rarest ones, contain one or more low-density $CO_2$ bubbles, as confirmed by Raman microspectroscopy (Fig. 2i). No daughter phases were found in any kind of melt inclusions, but in a few cases, heterogeneous trapping of plagioclase and apatite was observed; these crystals occupy almost all the space inside the inclusion.

## 5. Microthermometry of fluid and melt inclusions

### 5.a. Fluid inclusions

All the fluid inclusions observed are made up only of pure carbon dioxide, as confirmed by the instantaneous

Table 1. Microprobe analyses of homogenized melt inclusions

| Run | 35a-1 | 35a-2 | 35a-3 | 35a-4 | 35a-5 | 37a-1 | 37a-2 | 38-1 | 39a-1 | 41a | 42a | 43a | 43b | gl37b-1 | 41b | 42b | 42c |
|---|---|---|---|---|---|---|---|---|---|---|---|---|---|---|---|---|---|
| Th (°C) | 1100 | 1100 | 1100 | 1100 | 1100 | 1100 | 1100 | 1100 | 1107 | 1087 | 1100 | 1080 | 1080 | 1100 | 1087 | 1100 | 1100 |
| $SiO_2$ | 80.30 | 80.60 | 79.70 | 80.00 | 79.40 | 77.20 | 78.70 | 78.00 | 78.70 | 78.20 | 78.80 | 79.20 | 83.60 | 77.30 | 72.70 | 75.70 | 74.60 |
| $TiO_2$ | bdl | bdl | bdl | bdl | bdl | 0.03 | 0.04 | bdl | bdl | bdl | bdl | bdl | 0.03 | 0.03 | bdl | bdl | bdl |
| $Al_2O_3$ | 10.90 | 11.10 | 11.30 | 10.90 | 10.90 | 11.67 | 11.30 | 11.10 | 11.10 | 11.30 | 11.00 | 10.50 | 9.03 | 12.40 | 13.50 | 13.10 | 12.70 |
| $Fe_2O_3$ | 0.07 | 0.09 | 0.08 | 0.08 | 0.12 | 0.08 | 0.05 | 0.07 | 0.05 | 0.05 | 0.06 | 0.04 | 0.10 | 0.08 | 0.21 | 0.16 | 0.17 |
| FeO | 0.14 | 0.18 | 0.16 | 0.16 | 0.23 | 0.15 | 0.11 | 0.15 | 0.10 | 0.09 | 0.12 | 0.07 | 0.19 | 0.15 | 0.41 | 0.32 | 0.33 |
| MnO | bdl | 0.05 | bdl | 0.04 | 0.04 | bdl | 0.05 | bdl | bdl | bdl | 0.05 | bdl | bdl | bdl | 0.10 | 0.07 | 0.08 |
| MgO | 0.12 | 0.10 | 0.10 | 0.12 | 0.17 | 0.15 | 0.14 | 0.14 | 0.07 | 0.10 | 0.15 | 0.01 | 0.03 | 0.29 | 0.77 | 0.74 | 0.69 |
| CaO | 1.42 | 1.69 | 1.66 | 1.40 | 1.64 | 1.77 | 1.90 | 0.24 | 0.37 | 1.81 | 1.76 | 0.29 | 0.42 | 2.20 | 4.33 | 3.37 | 3.38 |
| $Na_2O$ | 1.28 | 0.91 | 0.84 | 1.36 | 1.31 | 1.95 | 0.88 | 2.14 | 1.52 | 1.16 | 1.84 | 1.43 | 1.61 | 1.59 | 0.90 | 1.09 | 1.28 |
| $K_2O$ | 3.85 | 3.51 | 3.62 | 3.96 | 3.67 | 3.71 | 3.66 | 6.23 | 5.98 | 3.70 | 3.71 | 5.65 | 4.26 | 3.88 | 3.12 | 3.44 | 3.05 |
| $P_2O_5$ | 0.13 | 0.09 | 0.11 | 0.10 | 0.11 | 0.07 | 0.10 | bdl | bdl | 0.12 | 0.13 | 0.05 | bdl | bdl | 0.04 | 0.04 | 0.04 |
| SrO | 0.08 | 0.06 | bdl | bdl | bdl | 0.06 | bdl | bdl | 0.04 | bdl | 0.05 | bdl | 0.05 | 0.08 | 0.10 | bdl | 0.10 |
| BaO | 0.11 | bdl | 0.04 | bdl | 0.06 | bdl | bdl | bdl | bdl | bdl | bdl | bdl | bdl | bdl | bdl | bdl | bdl |
| Cl | bdl | bdl | 0.02 | 0.02 | bdl | 0.27 | 0.22 | 0.09 | 0.02 | 0.17 | 0.28 | 0.04 | 0.01 | 0.33 | 0.75 | 0.32 | 0.42 |
| Total | 98.21 | 98.32 | 97.61 | 98.14 | 97.61 | 97.07 | 97.15 | 98.18 | 97.93 | 96.74 | 97.90 | 97.28 | 99.28 | 98.25 | 96.83 | 98.36 | 96.74 |
| Fe no. | 0.40 | 0.50 | 0.47 | 0.43 | 0.44 | 0.36 | 0.30 | 0.37 | 0.44 | 0.34 | 0.31 | 0.80 | 0.78 | 0.23 | 0.23 | 0.20 | 0.21 |
| ASI | 1.47 | 1.65 | 1.69 | 1.42 | 1.46 | 1.33 | 1.61 | 1.06 | 1.19 | 1.52 | 1.30 | 1.21 | 1.18 | 1.41 | 1.54 | 1.54 | 1.51 |
| MALI | 0.10 | 0.07 | 0.07 | 0.10 | 0.09 | 0.11 | 0.07 | 0.20 | 0.17 | 0.08 | 0.11 | 0.16 | 0.13 | 0.09 | 0.02 | 0.05 | 0.05 |

All oxides are wt % (bdl – below detection limit). $Fe_2O_3$ is calculated considering $Fe_2O_3/FeO = 0.5$, as suggested by Middlemost (1989) for high silica rocks. Inclusions 41b, 42b and 42c are located close to rims of quartz grains.

melting process of frozen $CO_2$, occurring between $-56.7$ and $-56.5 \pm 0.1$ °C; Raman investigations detected no water peak. The density values of the fluid inclusions found range from 150 to 690 kg/m$^3$, corresponding to 41–334 MPa. Most of these values do not correspond to trapping conditions due to late re-equilibration processes, as suggested by the presence of a halo of very small bubbles and small cracks around the inclusions (Andersen & Neumann, 2001; Vityk & Bodnar, 1998). Nevertheless, it is possible to utilize these data to locate at least one possible magma storage area within the shallow crust. The hypothetical stratigraphic sequence at the islands of Vulcano and Lipari was used to calculate the depth of trapping or re-equilibration of the fluid inclusions. An average density of 2500 kg/m$^3$ was assumed for the 1 km thick volcanic pile, resting on a 2.1 km thick sedimentary cover, with an average density of 2600 kg/m$^3$, and in turn on a metamorphic pile of density 2720 kg/m$^3$ (Falsaperla *et al.* 1999; Barberi *et al.* 1994). Further details may be found in Zanon, Frezzotti & Peccerillo (2003).

The calculated depth of the trapping/re-equilibration interval of 1.7–4.7 km, resulting from the consideration of the influx of all the layers, should correspond to a magma storage area, located at the boundary between the sedimentary cover and the upper metamorphic crust. As for high-density fluid inclusions, it is only possible to assume that trapping of these probably occurred at a greater depth than 12.7 km below the surface.

### 5.b. Melt inclusions

Homogenization temperatures were measured through long-lasting runs by continuously checking, on a TV camera connected to the microscope, the disappearance of the small shrinkage bubble, as no daughter phases were found in the melt. Most inclusions homogenized in the range of 1080–1107 °C. Only a small (Ø < 5 μm) isolated inclusion, trapped in an opaque quartz grain, homogenized at 993 °C, after two hours of slow heating and was considered to be representative of a late-stage trapping event.

Attempts were made to develop shrinkage bubbles in the inclusions that were perfectly glassy and free of shrinkage bubbles, by repeatedly heating/quenching several inclusions, but these were unsuccessful. During these runs, inclusions were quickly heated to 1070 °C and quenched after 5 to 10 minutes. In other cases, temperature was quickly reduced, every 20 to 85 minutes, from 1200 °C to 1100 °C, by 15–50 °C each time. For these inclusions, it was assumed that they had the same range of homogenization temperatures measured for the inclusions containing shrinkage bubbles, due to their proximity and, sometimes, their belonging to the same trail.

Inclusions containing a small $CO_2$ bubble, with or without accidentally trapped phases (quartzes, feldspars, pyroxenes), normally started to melt at temperatures well above 1150 °C, with the resorption of the $CO_2$ bubble at a temperature of 1170–1200 °C, only in the case of tiny-sized bubbles. Finally, inclusions hosting mineral phases started to melt at temperatures above 1220 °C, and never attained complete homogenization. These high temperatures were not considered, as they exceeded the real range of homogenization temperatures.

## 6. Geochemistry

### 6.a. Xenoliths

The whole-rock geochemistry of the xenoliths is consistent with a quartz-based mineralogy; in Table 1,

Table 2. XRF and ICP-MS data of quartz-rich xenoliths from Monte dei Porri

| Name | SaMp4 | SaMp5 | SaMp13 | Eo98-8 |
|---|---|---|---|---|
| $SiO_2$ | 98.51 | 97.09 | 98.56 | 98.43 |
| $TiO_2$ | 0.01 | 0.01 | 0.01 | 0.01 |
| $Al_2O_3$ | 0.27 | 1.04 | 0.88 | 0.79 |
| $Fe_2O_{3tot}$ | 0.39 | 0.22 | 0.11 | 0.05 |
| MnO | 0.04 | 0.04 | 0.04 | 0.04 |
| MgO | 0.04 | 0.06 | 0.01 | 0.02 |
| CaO | 0.11 | 0.10 | 0.21 | 0.11 |
| $Na_2O$ | 0.49 | 0.44 | 0.06 | 0.07 |
| $K_2O$ | 0.04 | 0.05 | 0.06 | 0.07 |
| $P_2O_5$ | 0.01 | 0.01 | 0.01 | 0.01 |
| LOI | 0.09 | 0.94 | 0.00 | 0.38 |
| Total | 100.00 | 100.00 | 100.00 | 99.98 |
| Ba | 7 | 37 | bdl | 4.8 |
| Ce | 1.2 | 0.7 | 1.1 | 1.1 |
| Cr | 6 | 7 | 2 | 2 |
| Cu | 50.5 | 11 | 5.2 | 9.2 |
| Ga | 0.3 | 0.4 | 0.3 | 0.3 |
| Ge | 1.6 | 0.9 | 2.1 | 0.5 |
| Hf | bdl | 0.1 | bdl | 0.1 |
| La | 0.6 | 0.5 | 0.5 | 0.5 |
| Nb | bdl | 0.3 | 0.2 | 0.2 |
| Nd | 0.5 | 0.5 | 0.3 | 0.4 |
| Ni | 3 | 1 | bdl | bdl |
| Pb | 13 | 1 | 15 | 17 |
| Rb | 1.2 | 0.9 | 3.4 | 2.0 |
| Sm | 0.09 | 0.1 | 0.1 | bdl |
| Sr | bdl | 5 | bdl | 6 |
| Ta | bdl | 0.05 | 0.05 | bdl |
| Th | 0.1 | 0.2 | 1.1 | bdl |
| U | bdl | 0.1 | 0.4 | 0.3 |
| V | 10.9 | 2.2 | bdl | 2.0 |
| Y | 0.37 | 0.35 | 0.11 | 0.25 |
| Zr | 1 | 2 | 1 | 1 |

Major elements are wt %, minor and trace elements are ppm (bdl – below detection limit).

Table 2 and in the diagrams of Figure 3, silica is always between 97.0% and 98.6% and $Al_2O_3$ between 0.3% and 1.0%. Other oxides amount to less than 1%, with average values of $Fe_2O_3$, CaO and $Na_2O$ slightly over 0.1%.

Among trace elements, Ba, Cr, Cu, Pb and V exhibit, on average, the highest concentrations even if these are highly variable. High-field-strength elements (Hf, Nb, Ta, Th, U, Y and Zr) are low or sometimes below detection limit. REE are very low and very often below detection limit (commonly less than 0.5 ppm). Their concentrations are quite consistent in respect to those of the other elements, except for Ce concentrations which are higher (0.7–1.2 ppm).

A comparison with the primitive-mantle-normalized patterns of trace elements in the quartz-rich lithologies of the Calabro–Peloritani range (Frezzotti *et al.* 2004), illustrated in Figure 4a, shows a general depletion in almost all elements, although there are considerable variations in some of them, namely Ba, Th, Rb, U and to a lesser extent Y. These variations could be explained by the presence of small amounts of accessory phases, such as feldspar and zircon.

The chondrite-normalized REE pattern shown in Figure 4b is quite flat, with normalized concentrations of elements that are constantly within the range 0.2–2.7 times chondritic values.

### 6.b. Melt inclusions

The chemical composition of homogenized melt inclusions obtained by electron microprobe analysis is similar to that of a high-K rhyolite (Table 1), with silica contents of 72.7–83.6% and $K_2O$ of 2.4–6.2% (Fig. 3). This high silica content is a natural character of these melts, as already demonstrated by Clocchiatti *et al.* (1994), Renzulli *et al.* (2001), Vaggelli *et al.* (2003) and Frezzotti *et al.* (2004) for similar melt inclusions hosted in quartz-rich xenoliths form other Aeolian islands, and it is not the artificial result of the interference of the microprobe beam with the host quartz. Moreover, it is not possible to correlate the silica content of homogenized melt inclusions with the utilized spot size, not even for the smallest inclusions analysed ($\sim 10$ μm). Figure 5 shows that possible contamination with quartz during the homogenization process is to be excluded for inclusions that homogenize up to 1100 °C. These inclusions are characterized by a wide compositional variation in some oxides at the same temperature ($SiO_2$, $Al_2O_3$, MgO, CaO and $K_2O$), which cannot be referred to quartz contamination, because it is only a natural character of these melts. Experiments carried out by Becker, Holtz & Johannes (1998) on the Qz–Ab–Or $\pm$ $H_2O$ system, at 5 kbar and in a similar range of temperatures, obtained a melt with the same geochemical characteristics and mineral modal abundances.

The inclusions that homogenize at temperatures over 1150 °C have, on an average, higher contents of $SiO_2$ and lower alkalis or higher total iron, $Na_2O$, CaO and $P_2O_5$. These anomalous values are partially due to contamination with melts produced by the partial melting of tiny trapped phases (apatite, Na-feldspar and pyroxene) during the homogenization process or the melting of the host quartz. These perfectly transparent crystals were sometimes discovered through back-scattered electron imaging just before analysis. Due to these anomalies, however, the analyses carried out on inclusions homogenized at temperatures over 1150 °C were discarded and are not discussed further.

Homogenized inclusions exhibit the greatest variations in $SiO_2$, $Al_2O_3$, CaO and $Na_2O$ contents, as shown in Figure 3, where the compositions of melt trapped close to quartz rims are plotted in Harker diagrams and compared with inclusions trapped close to quartz cores. From petrographical evidence, early trapped inclusions (filled triangles) lie close to the core of the host crystal, while inclusions trapped close to the rim (empty triangles) are thought to represent the latest trapped composition in the history of the grain and, possibly, of the whole xenolith.

By comparing these two kinds of inclusions it is evident that late-stage trapped inclusions are

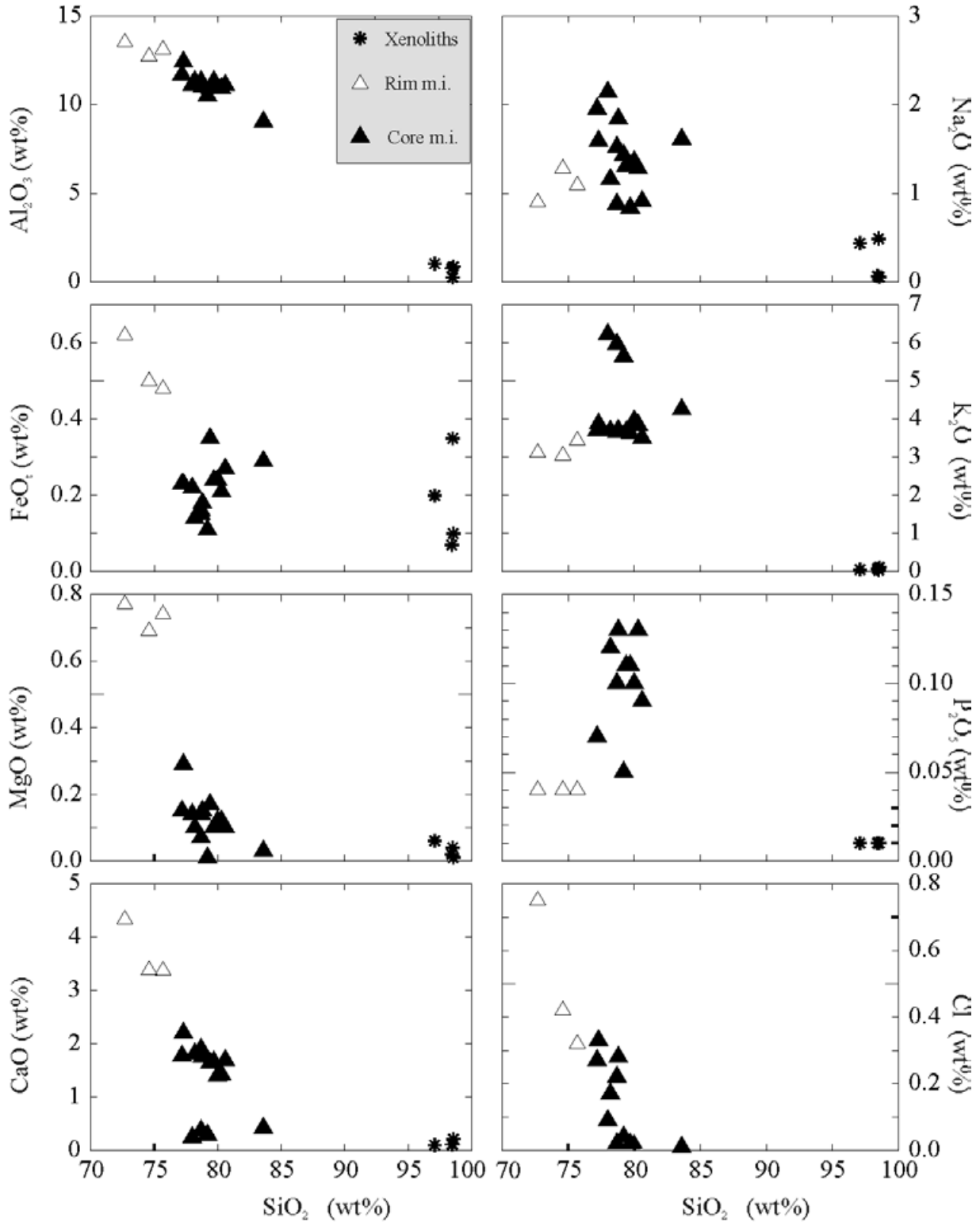


Figure 3. Variation diagrams for xenoliths and homogenized melt inclusions. Open triangles represent melt compositions found close to the rim of quartz crystals, while filled triangles are the melt compositions trapped close to the quartz cores. While xenoliths do not show any meaningful variation, due to the quartz-rich mineralogy, composition of melt inclusions shows some inter-elemental correlations.

characterized by higher contents of $Al_2O_3$ (12.7–13.5%), MnO (0.07–0.1%), MgO (0.7–0.8%) and CaO (3.4–4.3%) and, to some extent, total iron, while showing lower contents of $SiO_2$ (72.7–75.7%), alkali ($K_2O = 3.0$–$3.4$%; $Na_2O = 0.9$–$1.3$%) and $P_2O_5$ (0.04%).

The most striking features of early-stage trapped inclusions are the high values of $SiO_2$, consistently

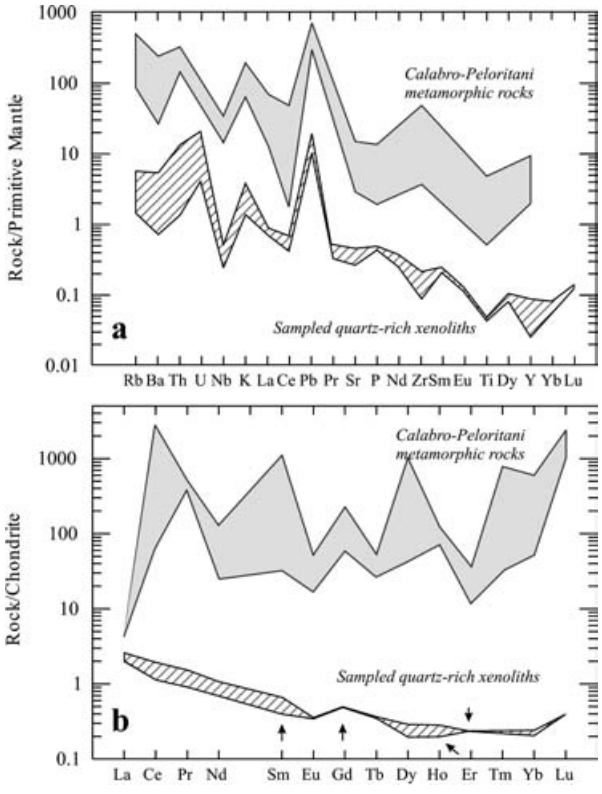


Figure 4. Spider diagrams of (a) trace elements and (b) REE of sampled xenoliths. Dashed areas are selected quartz-rich metamorphic rocks (gneisses, micaschists and granulites) of the Calabro-Peloritani range (Frezzotti *et al.* 2004). In (b), arrows indicate data of REE below detection limits.

above 77.3%, and $P_2O_5$ which shows no significant correlation with silica. CaO (0.2–2.2%) and $Al_2O_3$ are negatively correlated with $SiO_2$. Similar behaviour is exhibited by MgO (0.01–0.3%), though its negative correlation is less evident. $FeO_t$ clusters between 0.1 and 0.4 wt%, and these values are lower than those of external inclusions which form a small group ranging from 0.5 to 0.6%. Data on $Na_2O$ and $K_2O$ from all the inclusions form a cluster between 0.8–2.1% and 3.1–6.2%, respectively, with the external inclusions showing constant and lower values. $TiO_2$ and MnO concentrations are extremely low for both inclusions or below detection limit. Chlorine concentrations are negatively correlated with silica and are less than 0.8%, while external inclusions exhibit the highest values. Traces of BaO characterize inner inclusions ($\leq$ 1100 ppm), while the external ones show higher concentrations of SrO (1000 ppm compared to 400–800 ppm).

Finally, microprobe analyses gave totals close to 96.74–99.28 wt%, which suggested the possible presence of dissolved gas in the glass. Raman microspectrometry in melt inclusions confirmed the presence of water with a peak centred at 3550 $cm^{-1}$.

## 7. Discussion

### 7.a. Origin of xenoliths

Quartz-rich aggregates inside the basaltic andesites and andesites of Monte dei Porri are widespread as enclaves in these lavas, together with cumulus aggregates (commonly Cpx + Pl). Chondrite-normalized (Sun, 1980) and primitive mantle-normalized (Sun & McDonough, 1989) patterns of trace elements and REEs of Figure 4 discriminate between the pure metamorphic realm of the quartz-rich rocks of the Calabro–Peloritani range (Frezzotti *et al.* 2004) and the sampled xenoliths, so that it clearly appears that these xenoliths are not a metamorphic rock.

Similar quartz aggregates, found in the lavas of Alicudi, Vulcano and Stromboli and sometimes containing wollastonite and anorthite, were interpreted as quartz-bearing residues or 'restites' originated by some melting event that affected the deep crust below the arc (Crisci *et al.* 1991; Peccerillo & Wu, 1992; Renzulli *et al.* 2001; Zanon, Frezzotti & Peccerillo, 2003; Vaggelli *et al.* 2003).

Evidence of the origin of xenoliths may be found in the particular texture of these rocks, as shown in Figure 2, and in the highly refractory nature of their mineralogy, consisting almost exclusively of quartz (sometimes partially resorbed, especially near triple junctions) and exhibiting cristobalitic rims, which indicates the occurrence of thermal shock. Moreover, the presence of glassy and transparent intergranular films provides additional evidence that some melting process affected the original rock.

### 7.b. Classification and origin of melt inclusions

All the silicate melt inclusions trapped inside quartz grains have the same physico-chemical characteristics; the high content of $SiO_2$ and $K_2O$ makes these melts similar to a high-K ryholite. Ryholites are lacking among the volcanic products erupted from Monte dei Porri and during earlier volcanic cycles; this detail, coupled with the lack of daughter minerals in the melt, seems to exclude the hypothesis that a host basaltic–andesitic or andesitic magma generated the trapped melt through fractional crystallization.

Alternatively, these inclusions might represent the ultimate product of an anatectic process affecting some quartz-rich metamorphic rocks belonging to the Calabro–Peloritani range. The small amount of water inside the melt gives strength to this hypothesis. It may be assumed that the process of crustal melting was progressive, and this caused the production of various silicic melts and various restitic phases. Some of them were heterogeneously trapped in quartz, as confirmed by the presence of large-size crystals of feldspar and chloroapatite inside the melt inclusions.

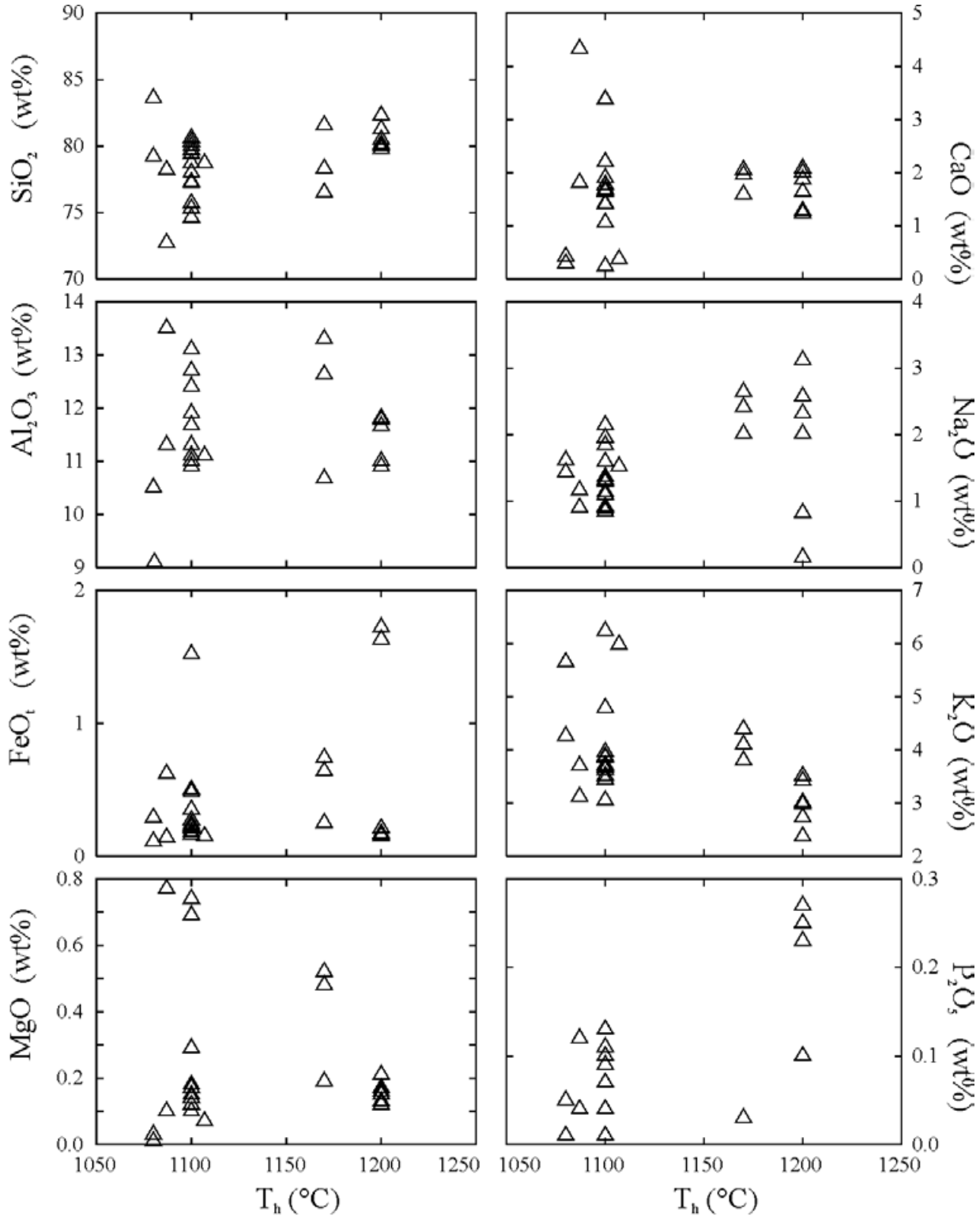


Figure 5. Diagrams showing variation of composition of melt inclusions with $T_h$. Inclusions which homogenized at temperatures above 1150 °C showed possible contamination with the host quartz and/or with accidentally trapped minerals such as plagioclase, pyroxene and apatite. These inclusions were therefore not taken into consideration.

Taking into account the observed chemical variations, it appears that the minerals involved in the melting process are mainly quartz and an Al–Na–K-bearing phase. The triangular plot of Figure 6 shows the composition of melts compared to that of the minerals that constitute quartz-rich metamorphic lithologies (Peccerillo & Wu, 1992; De Astis *et al.* 1997; Xie, Byerly & Ferrell, 1997; Biino & Gröning, 1998;

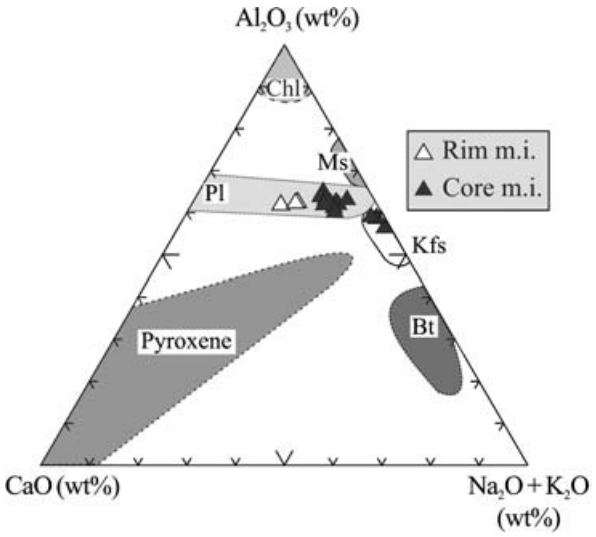


Figure 6. Triangular plot comparing compositions of trapped melt inclusions and analyses of the commonest minerals, constituting quartz-rich metamorphic lithologies. Symbols as in Figure 3. Filled areas represent compositional fields of different minerals: Bt – biotite; Chl – chlorite; Kfs – K-feldspar; Ms – muscovite; Pl – plagioclase. Oxides are in wt %. Melting of plagioclase seems to be the main reason for the observed composition of trapped melt.

Harlov & Wirth, 2000; Santo, 2000; Cruciani *et al.* 2001). The analysed melts fall in the field of those produced with plagioclase contribution and exclude mica (biotite or muscovite) as the main possible factor responsible for chemical variation, especially for the high content in $K_2O$ and the low MgO content. As to the possible role of K-feldspar in these melt production events, according to Carrington & Watt (1995), this phase may have played an active role during the first stage of anatexis in water-undersaturated conditions, while biotite did not participate. According to Clemens, Droop & Stevens (1997), this event affected the deep crust. Later, biotite broke down, increasing the $H_2O/K_2O$ ratio and producing the characteristic pattern shown in Figure 6. This event probably occurred at a shallower level in the crust (Clemens, Droop & Stevens, 1997).

A possible key to understanding the origin of these silicic melts is the major-element-based classification scheme proposed by Frost *et al.* (2001). In Figure 7, different binary plots indicate the variation of the suggested parameters for silica as compared with the fields of dacites, rhyodacites and rhyolites from several islands of the arc (data from Esperança *et al.* 1992; Gertisser & Keller, 2000; Calanchi *et al.* 2002 and De Astis *et al.* 1997). Figure 7a shows that these melts are all peraluminous, with an Aluminium Saturation Index $> 1$ (ASI: Shand, 1943). The progressive increase in alumina and calcium contents (Figs 3, 7a) and the slight decrease in alkalis may indicate an

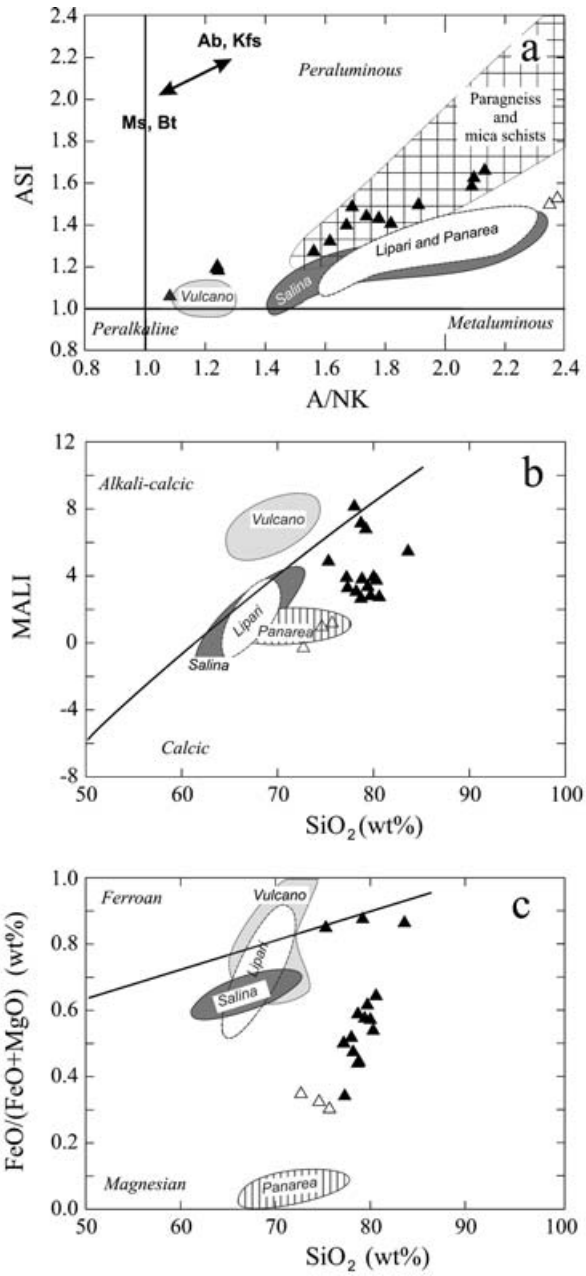


Figure 7. Classification scheme proposed by Frost *et al.* 2001 for granitoid melts. (a) ASI v. A/NK (Shand, 1943) diagram for analysed melt inclusions. ASI is calculated as molecular ratio Al/(Ca-1.67P + Na + K) (Shand, 1943) and A/NK as Al/(Na + K). Area with square hatching represents the field of muscovite-bearing micaschists and paragneiss of the Calabro–Peloritani range (Crisci *et al.* 1982; Rottura *et al.* 1991; Frezzotti *et al.* 2004); areas representing dacites and rhyolites of the different islands are also drawn (De Astis *et al.* 1997; Gertisser & Keller, 2000; Calanchi *et al.* 2002; Gioncada *et al.* 2003; De Rosa *et al.* 2003). Ab – albite; other abbreviations as in Figure 6. (b) MALI v. $SiO_2$ diagram discriminating between calcic and alkali-calcic fields. MALI (Modified Alkali-Lime Index) is calculated according to Frost *et al.* (2001) as molecular $Na_2O + K_2O$–CaO. (c) Fe no. v. $SiO_2$ diagram discriminating between ferroan and magnesian field. Fe no. is calculated as molecular FeO/(FeO + MgO).

involvement in the melting process of progressively more anorthite-rich plagioclase, as shown also by the composition of late trapped melts in the diagram of Figure 7b, where the Modified Alkali-Lime Index (MALI: Frost *et al.* 2001), plotted against $SiO_2$, again shows a progressive increase in CaO and a slight reduction in $SiO_2$ in late trapped melts. Due to its more refractory nature, melting of anorthite should imply an increase in the degree of melting, higher temperature and a reduced content of dissolved water in the melt. This latter condition seems to be probable in the first stages of the melting process.

Finally, Figure 7c illustrates the magnesian character of these melt inclusions, although it must be considered that the contents of MgO and FeO are extremely low.

Melting experiments performed by Holtz & Johannes (1991) and Patiño-Douce & Harris (1998) on biotite-bearing gneisses and micaschists at temperatures above 800 °C generated peraluminous water-undersaturated rhyolitic melts according to the following reaction:

$$\text{Bt} + \text{Qz} + \text{Pl} = \text{Opx} + \text{Fe–Ti oxides} + \text{melt}$$

This reaction justifies the low content of MgO and FeO, the high ASI numbers (Table 1) of melt inclusions and the small amount of water. In contrast, pyroxenes and Fe–Ti oxides were never found in the quartz-rich xenoliths from the islands of Alicudi and Vulcano (Frezzotti *et al.* 2004; Bonelli *et al.* in press). This could be explained by the small number of these phases participating in further melting processes, thus contributing to the small quantities of Fe and Mg, or by their gravitational fractionation. In both cases, these xenoliths could indicate the late stage of crustal melting of a depleted metamorphic rock. It therefore seems evident that the peraluminous character of the melt is due only to the contribution of feldspar.

Among the accessory phases, the most remarkable role was played by chlorapatite, whose contribution seems evident in the higher Cl content of late-stage melt inclusions. However, the small content of phosphorus indicates only a secondary role for this phase.

As to the presence of the carbon dioxide trapped inside quartz grains, there is room only for some speculation. Its solubility into a high-silica melt is extremely low (e.g. Fogel & Rutherford, 1990; Holloway, Pan & Gudmundsson, 1992; Blank, Stolper & Carroll, 1993), and no peak related to dissolved $CO_2$ in silicate inclusions was detected through Raman microspectroscopy. In any case, the presence of multiple small $CO_2$ bubbles of very low density inside some melt inclusions of noteworthy size seems to indicate a degassing process which occurred at shallower depths, while single-bubble-trapping of higher density could represent a random contemporaneous trapping event of two immiscible phases, in which uprising gas could be the response to local phenomena within the host rock (Clemens & Droop, 1998) at a depth of more than 12.7 km.

To obtain more information on the origin of carbon dioxide, accurate investigations of oxygen and carbon isotopes are clearly necessary. In the absence of this information, it is only possible to exclude the presence, within the deep crust, of some shale layers acting as a possible source; on the other hand, one may hypothesize a mantle source for this fluid, as for mixed $CO_2$, $CO + N_2$ fluid inclusions in the quartz-rich xenoliths from the island of Alicudi (Bonelli *et al.* in press), which show extremely high density values, matching those at the Moho discontinuity.

Finally, according to Clemens, Droop & Stevens (1997) and Clemens & Droop (1998), carbon dioxide played no role during the generation of these high-silica, peraluminous melts.

No $H_2O$ fluid inclusions have been found in this kind of xenolith anywhere in the islands of the Aeolian archipelago. Clocchiatti *et al.* (1994) reported very low-density saline water inclusions in quartz-rich xenoliths at La Fossa di Vulcano (Vulcano Island) and related them to trapping episodes in the shallower hydrothermal reservoir. Consequently, it seems that no free water accompanied the uprising of these xenoliths.

Using Raman spectroscopy, a weak water peak was later detected, dissolved in trapped melt. According to several authors (e.g. Holtz & Johannes, 1991; Carrington & Watt, 1995; Clemens, Droop & Stevens, 1997; Becker, Holtz & Johannes, 1998; Patiño-Douce & Harris, 1998; Johnson *et al.* 2003), who studied melting in the Qz–Ab–Or ± fluids system, water-undersaturated rhyolitic melts are probably the first products of the anatexis of biotite-bearing quartzo-feldspathic rocks, due to the breakdown of K-feldspar. By increasing the degree of melting or the temperatures, biotite breaks down instead of K-feldspar, producing melts that are more and more water-saturated. In conclusion, all the observed characteristics and the absence of biotite as a restitic phase imply that these melt inclusions were produced during melting incongruent reactions, consuming biotite and producing small amounts of melt (2–5 vol.%) (Kriegsman, 2001).

The rocks composing the stratigraphy below the archipelago show various grades of metamorphism (from phyllites to granulites) and consist for the most part of high-grade rocks (micaschists and gneisses). Among the latter rocks, those that are most suitable as source rocks should be both peraluminous and composed of a mineralogical assemblage which is consistent with the geochemistry of melt inclusions (Chappel, 1999). In Figure 7a the composition of the melt inclusions matches that of peraluminous metamorphic rocks such as paragneiss and micaschists; however, due to the fact that the melting process affected a large area of the basement and occurred

repeatedly in the history of the Salina Island, it is not possible to exclude other quartz- and feldspar-bearing rocks as possible source rocks (acid granulites).

The similarities with high-K rhyolites cropping out in many islands of the arc may suggest a common origin through this anatectic process; in other words, it may be justified to consider that the rhyolites erupted by the different volcanoes throughout the archipelago were perhaps generated by crustal melting processes occurring below this area (Barker, 1987; Crisci *et al.* 1991; Esperança *et al.* 1992). In reality, even though both the melt inclusions and the Aeolian rhyolites show similar $SiO_2$ and $K_2O$ contents, it is not likely that they originated from the same process. Figure 7 shows that the analysed melt inclusions are substantially different, not only from the rhyolites of Salina itself (Gertisser & Keller, 2000), but also from the other silica-rich lavas of the other islands of the archipelago, clearly suggesting a different genetic process.

Moreover, the very low water content and the high average viscosity of these melt inclusions ($10^{4.9}$ Pa × s, calculated from Bottinga & Weill, 1972) make the possible ascent from the source quite difficult. Thus, it is not possible to hypothesize that the silica-rich magmatism in the island of Salina was generated by the eruption of the same batches of $SiO_2$-rich liquids trapped as melt inclusions.

### 7.c. Xenolith ascent path

The microthermometry of fluid inclusions, the geochemistry of melt inclusions and the study of the microstructure and texture of the xenoliths can help to trace back the history of these rocks and, consequently, to acquire more information and to locate the magma ascent path, through which these crustal fragments were carried upwards, at Monte dei Porri.

The quartz-rich xenoliths of Monte dei Porri formed in the deep crust (> 12.7 km); this may be deduced from analogies with the textural characteristics of the xenoliths of Vulcano Island and from the barometric conditions of re-equilibration of $CO_2$ fluid inclusions (Fig. 8). The original lithology of this area experienced several crustal melting and partial melt extraction events, with the consequent generation of rock layers composed of quartz-rich residues showing pores filled with the most recent anatectic melt.

Intruding magma dragged some fragments of this country rock toward the surface. Xenolith-bearing magma rose quickly through the crust to the shallower resting area (1.3–2.8 km), as indicated by the total resetting of high-density fluid inclusions (Fig. 8) and the trapping of some fluid inclusions of low-density $CO_2$.

It is still being debated whether these melting processes were generated by the rise of geotherms, caused by the onset of the first stage of Aeolian magmatism, as suggested by Crisci *et al.* (1991), or

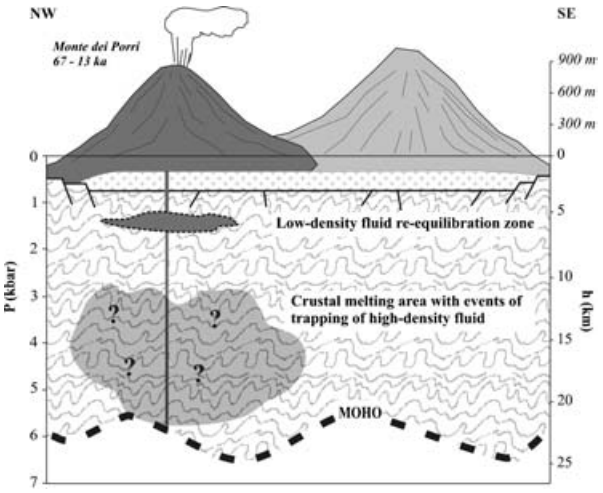


Figure 8. Sketch of the possible magma ascent path beneath Monte dei Porri. Height of the volcanoes is exaggerated. Due to the scarcity of data on high-density fluid inclusions, it was impossible to locate a deeper magma reservoir.

by prolonged contact between basaltic magma and country rock inside intracrustal reservoirs located at a greater depth than 12.7 km, as also confirmed by the structural data on clinopyroxene (Nazzareni *et al.* 2001). It remains unclear whether contamination by these anatectic melts was responsible for the same geochemical features observed in all the Aeolian magmas (Esperança *et al.* 1992; Ellam *et al.* 1989; Ellam & Harmon, 1990; De Astis *et al.* 1997, 2000). The great differences in viscosity, thermal and chemical diffusion coefficients between these highly silicic melts and the host magma and the small amounts of produced anatectic melt may exclude this hypothesis (Grasset & Albarede, 1994; Poli, Tommasini & Halliday, 1996). Moreover, Tommasini & Poli (1992) stated that interaction processes between a static silicic melt and an intruding basic or intermediate host magma are only possible at the boundary between these two melts. Finally, Frezzotti *et al.* (2004) demonstrated that the assimilation process of the silicic melt trapped in quartz-rich xenoliths at Vulcano Island cannot explain the geochemical characteristics observed in the host magma.

## 8. Conclusions

Quartz-rich xenoliths from Monte dei Porri contain numerous melt inclusions, whose geochemistry corresponds to that of a high-alumina, high-potassium silicic melt, produced during the late stages of the crustal melting of high-grade metamorphic rocks with a mineralogical assemblage represented by Qz + Kfs + (Na–Ca) Pl + Bt ± accessory phases. Anatexis repeatedly affected different fractions of the metamorphic pile, sometimes in the presence of free carbon dioxide, causing the random generation of $CO_2$-bubble-bearing and bubble-free melts. The observed small-scale compositional variations are due to differential participation

of mineralogical phases and various degrees of melting or higher temperatures. The peraluminous character of these melts may reflect the main role of plagioclase in the melting process, especially during the latest stages. The batches of melt produced at different times are more and more enriched in Ca and depleted in alkalies; this suggests the progressive dissolution of anorthite and K-feldspar and the shifting toward $H_2O$-saturated conditions caused by the breakdown of biotite. In conclusion, it is possible that this process occurred progressively, including different melting events, starting from a fertile metamorphic rock and ending up with a rock with a strong residual character (more and more quartz-rich assemblages). The range of homogenization temperatures (990–1107 °C) seems to confirm this hypothesis.

Bubbles of carbon dioxide, trapped as fluid inclusions, indicate the presence of a magma buoyancy layer within the range ~40–145 MPa, thus suggesting the presence of a geological discontinuity of regional importance, as already indicated by studies on fluid inclusions for other Aeolian Islands (Zanon, Frezzotti & Peccerillo, 2003; Bonelli *et al.* in press; Vaggelli *et al.* 2003). This discontinuity may represent the transition from the sedimentary cover to the metamorphic pile; it could hinder the rise of magma and consequently favour the formation of reservoirs.

**Acknowledgements.** The authors wish to acknowledge the assistance provided by W. Lustenhouwer during the microprobe analyses and W. Koot for the use of polishing facilities (both at the Vrije Universiteit, Amsterdam). M. L. Frezzotti and A. Peccerillo provided a great contribution to the final discussion, while D. M. Pyle and R. Gertisser improved this work significantly with their reviews. Finally, the research on the Aeolian arc and on the Italian recent and active volcanism was supported by C.N.R. (the Italian organization for scientific research) and by local projects carried out by the Universities of Perugia and Amsterdam. Raman analytical facilities were provided by P.N.R.A. (the Italian organization for research in Antarctica). Igor Nikogosian was supported by NWO (ALW–810.31.002) and ISES (Netherlands Research Centre for Integrated Solid Earth Science).

## References

ANDERSEN, T. & NEUMANN, E. R. 2001. Fluid inclusions in mantle xenoliths. *Lithos* **55**, 301–20.

BARBERI, F., GANDINO, A., GIONCADA, A., LA TORRE, P., SBRANA, A. & ZENUCCHINI, C. 1994. The deep structure of the Eolian arc (Filicudi-Panarea-Vulcano sector) in light of gravity, magnetic and volcanological data. *Journal of Volcanology and Geothermal Research* **61**, 189–206.

BARKER, D. S. 1987. Rhyolites contaminated with metapelite and gabbro, Lipari, Aeolian Islands, Italy: products of lower crustal fusion or of assimilation plus fractional crystallization? *Contributions to Mineralogy and Petrology* **97**, 460–72.

BECKER, A., HOLTZ, F. & JOHANNES, W. 1998. Liquidus temperatures and phase compositions in the system Qz–Ab–Or at 5 kbar and very low water activities. *Contributions to Mineralogy and Petrology* **130**, 213–24.

BIINO, G. G. & GRÖNING, P. 1998. Cleavage mechanism and surface chemical characterization of phengitic Muscovite and Muscovite as constrained by X-Ray Photoelectron Spectroscopy. *Physics and Chemistry of Minerals* **25**(2), 168–81.

BLANK, J. G., STOLPER, E. M. & CARROL, M. R. 1993. Solubilities of carbon dioxide and water in rhyolitic melt at 850 °C and 750 bars. *Earth and Planetary Science Letters* **119**, 27–36.

BONELLI, R., FREZZOTTI, M. L., ZANON, V. & PECCERILLO, A. In press. Evolution of the volcanic plumbing system of Alicudi (Aeolian Island): evidence from fluid inclusions in quartz xenoliths. *Annales Geophysicae*.

BOTTINGA, Y. A. & WEILL, D. F. 1972. The viscosity of magmatic silicate liquids: a model for calculation. *American Journal of Science* **272**, 438–73.

CALANCHI, N., PECCERILLO, A., TRANNE, C. A., LUCCHINI, F., ROSSI, P. L., KEMPTON, P., BARBIERI, M. & WU, T. W. 2002. Petrology and geochemistry of volcanic rocks from the island of Panarea: implications for mantle evolution beneath the Aeolian island arc (southern Tyrrhenian sea). *Journal of Volcanology and Geothermal Research* **115**, 367–95.

CARMINATI, E., WORTEL, M. J. R., SPAKMAN, W. & SABADINI, R. 1998. The role of slab detachment processes in the opening of the Western-Central Mediterranean basins: some geological and geophysical evidence. *Earth and Planetary Science Letters* **160**, 651–65.

CARRINGTON, D. P. & WATT, G. R. 1995. A geochemical and experimental study of the role of K-feldspar during water-undersaturated melting of metapelites. *Chemical Geology* **122**, 59–76.

CHAPPEL, B. W. 1999. Aluminium saturation in I- and S-type granites and the characterization of fractionated haplogranites. *Lithos* **46**, 535–51.

CLEMENS, J. D. & DROOP, G. T. R. 1998. Fluids, P–T paths and fates of anatectic melts in the Earth's crust. *Lithos* **44**, 21–36.

CLEMENS, J. D., DROOP, G. T. R. & STEVENS, G. 1997. High-grade metamorphism, dehydrations and crustal melting: a reinvestigation based on new experiments in the silica-saturated portion of the system $KAlO_2$–MgO–$SiO_2$–$H_2O$–$CO_2$ at $P \leq 1.5$ GPa. *Contributions to Mineralogy and Petrology* **129**, 308–25.

CLOCCHIATTI, R., DEL MORO, A., GIONCADA, A., JORON, J. L., MOSBAH, M., PINARELLI, L. & SBRANA, A. 1994. Assessment of a shallow magmatic system: the 1888–90 eruption, Vulcano Island, Italy. *Bulletin of Volcanology* **56**, 466–86.

CRISCI, G. M., DE ROSA, R., ESPERANÇA, S., MAZZUOLI, R. & SONNINO, M. 1991. Temporal evolution of a three component system: the island of Lipari (Aeolian Arc, southern Italy). *Bulletin of Volcanology* **53**, 207–21.

CRISCI, G. M., DONATI, G., MESSINA, A., RUSSO, S. & PERRONE, V. 1982. L'unità superiore dell'Aspromonte. Studio geologico e petrografico. *Rendiconti della Società Italiana di Mineralogia e Petrologia* **38**(3), 989–1014.

CRUCIANI, G., FRANCESCHELLI, M., CAREDDA, A. M. & CARCANGIU, G. 2001. Anatexis in the Hercynian basement of NE Sardinia, Italy: a case study of the migmatite of Porto Ottiolu. *Mineralogy and Petrology* **71**(3–4), 195–233.

De Astis, G., La Volpe, L., Peccerillo, A. & Civetta, L. 1997. Volcanological and petrological evolution of Vulcano island (Aeolian Arc, southern Tyrrhenian Sea). *Journal of Geophysical Research* **102**, 8021–50.

De Astis, G., Peccerillo, A., Kempton, P. D., La Volpe, L. & Wu, T. W. 2000. Transition from calc-alkaline to potassium-rich magmatism in subduction environments: geochemical and Sr, Nd, Pb isotopic constraints from the island of Vulcano (Aeolian arc). *Contributions to Mineralogy and Petrology* **136**, 684–703.

De Rosa, R., Donato, P., Gioncada, A., Masetti, M. & Santacroce, R. 2003. The Monte Guardia eruption (Lipari, Aeolian Islands): an example of a reversely zoned magma mixing sequence. *Bulletin of Volcanology* **65**, 530–43.

Ellam, R. M. & Harmon, R. S. 1990. Oxygen isotope constraints on the crustal contribution to the subduction-related magmatism of the Aeolian Islands, Southern Italy. *Journal of Volcanology and Geothermal Research* **44**, 105–22.

Ellam, R. M., Hawkesworth, C. J., Menzies, M. A. & Rogers, N. W. 1989. The volcanism of Southern Italy: role of subduction and the relationship between potassic and sodic alkaline magmatism. *Journal of Geophysical Research* **94**, 4589–601.

Esperança, S., Crisci, G. M., De Rosa, R. & Mazzuoli, R. 1992. The role of the crust in the magmatic evolution of the Island of Lipari (Aeolian Islands, Italy). *Contributions to Mineralogy and Petrology* **112**, 450–62.

Fabbri, A., Ghisetti, F. & Vezzani, L. 1980. The Peloritani–Calabria Range and the Gioia basin in the Calabrian Arc (Southern Italy): relationships between land and marine data. *Geologica Romana* **19**, 131–50.

Falsaperla, S., Lanzafame, G., Longo, V. & Spampinato, S. 1999. Regional stress field in the area of Stromboli (Italy): insight into structural data and crustal tectonic earthquakes. *Journal of Volcanology and Geothermal Research* **88**, 147–66.

Fogel, R. A. & Rutherford, M. J. 1990. The solubility of carbon dioxide in rhyolitic melts: a quantitative FTIR study. *American Mineralogist* **75**, 1311–26.

Francalanci, L. & Santo, A. P. 1993. Magmatological evolution of Filicudi volcanoes, Aeolian Islands, Italy: constraints from mineralogical, geochemical and isotopic data. *Acta Vulcanologica* **3**, 203–27.

Francalanci, L., Taylor, S. R., McCulloch, M. T. & Woodhead, J. D. 1993. Geochemical and isotopic variations in the calc-alkaline rocks of Aeolian Arc, southern Tyrrhenian Sea, Italy: constraints on magma genesis. *Contributions to Mineralogy and Petrology* **113**, 300–13.

Franzini, M. & Leoni, M. 1972. A full matrix correction in X-ray Fluorescence analysis of rock samples. *Atti della Società Toscana di Scienze Naturali* **73**, 7–22.

Frezzotti, M. L., Peccerillo, A., Zanon, V. & Nikogosian, I. 2004. Silica-rich melts in quartz xenoliths from Vulcano Island and their bearing on processes of crustal anatexis and crust-magma interaction beneath the Aeolian Arc, southern Italy. *Journal of Petrology* **45**, 3–26.

Frost, B. R., Barnes, C. G., Collins, W. J., Arculus, R. J., Ellis, D. J. & Frost, C. D. 2001. A geochemical classification for granitic rocks. *Journal of Petrology* **42**, 2033–48.

Gertisser, R. & Keller, J. 2000. From basalt to dacite: origin and evolution of the calc-alkaline series of Salina, Aeolian Arc, Italy. *Contributions to Mineralogy and Petrology* **139**, 607–26.

Gioncada, A., Mazzuoli, R., Bisson, M. & Pareschi, M. T. 2003. Petrology of volcanic products younger than 42 ka on the Lipari-Vulcano complex (Aeolian Islands, Italy): an example of volcanism controlled by tectonics. *Journal of Volcanology and Geothermal Research* **122**, 191–220.

Grasset, O. & Albarede, F. 1994. Hybridization of mingling magmas with different densities. *Earth and Planetary Science Letters* **121**, 327–32.

Harlov, D. E. & Wirth, R. 2000. K-feldspar-quartz and K-feldspar-plagioclase phase boundary interactions in garnet-orthopyroxene gneisses from the Val Strona di Omegna, Ivrea-Verbano Zone, northern Italy. *Contributions to Mineralogy and Petrology* **140**, 148–62.

Holloway, J. R. 1981. Compositions and volumes of supercritical fluids in the earth's crust. In *MAC Short Course in Fluid Inclusions* (eds L. S. Hollister and M. L. Crawford), pp. 13–38. Mineralogical Association of Canada.

Holloway, J. R., Pan, V. & Gudmundsson, G. 1992. High-pressure fluid-absent melting experiments in the presence of graphite: oxygen fugacity, ferric/ferrous ratio and dissolved $CO_2$. *European Journal of Mineralogy* **4**, 105–14.

Holtz, F. & Johannes, W. 1991. Genesis of peraluminous granites I. Experimental investigation of melt composition at 3 and 5 kb and various $H_2O$ activities. *Journal of Petrology* **32**, 935–58.

Honnorez, J. & Keller, J. 1968. Xenolithe in vulkanischen Gesteinen der Äolischen Inseln (Sizilien). *Geologische Rundschau* **57**(3), 719–36.

Hyppolite, J., Angelier, J. & Roure, F. 1994. A major change revealed by Quaternary stress patterns in the Southern Apennines. *Tectonophysics* **230**, 199–210.

Johnson, T. E., Gibson, R. L., Brown, M., Buick, I. S. & Cartwright, I. 2003. Partial melting of metapelitic rocks beneath the Bushveld Complex, South Africa. *Journal of Petrology* **44**, 789–813.

Kaye, M. J. 1965. X-ray fluorescence determinations of several trace elements in some standard geochemical samples. *Geochimica et Cosmochimica Acta* **29**, 139–42.

Keller, J. 1974. Petrology of some volcanic rock series of the Aeolian Arc, southern Tyrrhenian Sea: calc-alkaline and shoshonitic associations. *Contributions to Mineralogy and Petrology* **46**, 29–47.

Kriegsman, L. M. 2001. Partial melting, partial melt extraction and partial back reaction in anatectic migmatites. *Lithos* **56**, 75–96.

Lanzafame, G. & Bousquet, J. C. 1997. The Maltese escarpment and its extension from Mt. Etna to the Aeolian Islands (Sicily): importance and evolution of a litosphere discontinuity. *Acta Vulcanologica* **9**(1/2), 113–20.

Middlemost, E. A. K. 1989. Iron oxidation ratios, norms and the classification of volcanic rocks. *Chemical Geology* **77**, 19–26.

Milano, G., Vilardo, G. & Luongo, G. 1994. Continental collision and basin opening in Southern Italy: a new plate subduction in the Tyrrhenian Sea? *Tectonophysics* **230**, 249–64.

NAZZARENI, S., MOLIN, G., PECCERILLO, A. & ZANAZZI, P. F. 2001. Volcanological implications of crystal-chemical variations in clinopyroxenes from the Aeolian Arc, Southern Tyrrhenian Sea (Italy). *Bulletin of Volcanology* **63**, 73–82.

PATIÑO-DOUCE, A. E. & HARRIS, N. 1998. Experimental constraints on Himalayan anatexis. *Journal of Petrology* **39**, 689–710.

PECCERILLO, A. & WU, T. W. 1992. Evolution of calc-alkaline magmas in continental arc volcanoes: evidence from Alicudi, Aeolian arc (southern Tyrrhenian Sea, Italy. *Journal of Petrology* **33**, 1295–1315.

POLI, G., TOMMASINI, S. & HALLIDAY, A. N. 1996. Trace elements and isotopic exchange during acid-basic magma interaction processes. *Transactions of the Royal Society of Edinburgh, Earth Sciences* **87**, 225–32.

RENZULLI, A., SERRI, G., SANTI, P., MATTIOLI, M. & HOLM, P. M. 2001. Origin of high-silica liquid at Stromboli volcano (Aeolian Islands, Italy) inferred from crustal xenoliths. *Bulletin of Volcanology* **62**, 400–19.

ROTTURA, A., DEL MORO, A., PINARELLI, L., PETRINI, R., PECCERILLO, A., CAGGIANELLI, A., BARGOSSI, G. M. & PICCARRETA, G. 1991. Relationships between intermediate and acidic rocks in orogenic granitoids suites: petrological, geochemical and isotopic (Sr, Nd, Pb) data from Capo Vaticano (southern Calabria, Italy). *Chemical Geology* **92**, 153–76.

SANTO, A. 2000. Volcanological and geochemical evolution of Filicudi (Aeolian Islands, south Tyrrhenian Sea, Italy). *Journal of Volcanology and Geothermal Research* **96**, 79–101.

SHAND, S. J. 1943. *The eruptive rocks*. 2nd ed. New York: John Wiley, 444 pp.

SOBOLEV, A. V. & SLUTSKII, A. B. 1984. Composition and crystallisation conditions of the initial melt of the Siberian meimechites in relation to the general problem of ultrabasic magmas. *Soviet Geology and Geophysics* **25**, 93–104.

SUN, S. S. 1980. Lead isotopic study of young volcanic rocks from mid-ocean ridges, ocean islands and island arcs. *Philosophical Transactions of the Royal Society* **A297**, 409–45.

SUN, S.-S. & MCDONOUGH, W. F. 1989. Chemical and isotopic systematics of oceanic basalts: implications for mantle composition and processes. In *Magmatism in the Ocean Basins* (eds A. D. Saunders and M. J. Norry), pp. 313–45. Geological Society of London, Special Publication no. 42.

TOMMASINI, S. & POLI, G. 1992. Petrology of the Late-Carboniferous Punta Falcone gabbroic complex, northern Sardinia, Italy. *Contributions to Mineralogy and Petrology* **110**, 16–32.

VAGGELLI, G., FRANCALANCI, L., RUGGIERI, G. & TESTI, S. 2003. Persistent polybaric rests of calc-alkaline magmas at Stromboli volcano, Italy: pressure data from fluid inclusions in restitic quartzite nodules. *Bulletin of Volcanology* **65**, 385–404.

VAN DIJK, J. P. & SCHEEPERS, P. J. J. 1995. Neotectonic rotations in the Calabrian Arc: implications for a Pliocene–Recent geodynamic scenario for the central Mediterranean. *Earth Science Review* **39**, 207–46.

VITYK, M. O. & BODNAR, R. J. 1998. Statistical microthermometry of synthetic fluid inclusions in quartz during decompression reequilibration. *Contributions to Mineralogy and Petrology* **132**, 149–62.

XIE, X., BYERLY, G. R. & FERRELL, R. E. JR. 1997. IIb trioctahedral chlorite from the Barberton greenstone belt: crystal structure and rock composition constraints with implications for geothermometry. *Contributions to Mineralogy and Petrology* **126**, 275–91.

ZANON, V., FREZZOTTI, M. L. & PECCERILLO, A. 2003. Magmatic feeding system and crustal magma accumulation beneath Vulcano Island (Italy): evidence from fluid inclusions in quartz xenoliths. *Journal of Geophysical Research* **108**, 2298–301.